

Co₃V₂O₈ Composite Carbon Hollow Spheres Bidirectionally Catalyze the Conversion of Lithium Polysulfide to Improve the Capacity of Lithium-Sulfur Batteries

Jiangnan Zhang,^[a] Mingjun Xiao,*^[a, b] Wei Du,^[a] Jiawei Feng,^[a] Qiang Xiang,^[a] Yanshuang Meng,^[a, b] and Fuliang Zhu*^[a, b]

Although lithium-sulfur batteries have a high theoretical energy density that is higher than lithium-ion batteries, their development is limited by the slow kinetics of lithium polysulfide conversion. In this research, we utilize the excellent bidirectional catalysis and adsorption of lithium polysulfide by the bimetallic oxide Co₃V₂O₈ composite carbon hollow sphere to address the kinetic obstacle of lithium-sulfur battery. On the one hand, the carbon hollow sphere substrate provides a cavity that can hold a large amount of sulfur. On the other hand, it can limit the diffusion of lithium polysulfide by van der Waals forces. The combination of the above two points improves the

capacity and stability of lithium-sulfur batteries. It has a specific capacity of 1237.2 mAh g⁻¹ at 0.2 C current density and retains 603 mAh g⁻¹ after 100 cycles. At a high current density of 2 C, the specific capacity is 976.2 mAh g⁻¹. After 1000 cycles, it holds at 338.3 mAh g⁻¹, and the capacity retention rate per cycle is 99.89%. This work discovers the new potential of Co₃V₂O₈ as an electrocatalyst and proposes a process that can widely prepare carbon materials with complex uniform distribution of electrocatalysts to achieve high specific capacity of lithium-sulfur batteries.

1. Introduction

With the rapidly increasing demands for power batteries, mobile smart devices, aerospace, and other fields, traditional commercial lithium-ion batteries (LIBs) are hard to meet these demands.^[1–5] Therefore, developing a new battery system with high specific energy is necessary. Among the available types of next-generation batteries, lithium metal has the highest theoretical specific capacity (3860 mAh g⁻¹) and the lowest electrochemical potential (−3.04 V).^[6–9] At the same time, cathode sulfur reacts with anode lithium and undergoes a 16 electron transfer reaction, which depicts a high theoretical specific capacity of 1675 mAh g⁻¹ and a theoretical specific energy of 2550 Wh kg⁻¹. So, the lithium-sulfur (Li–S) batteries are considered promising candidates, which is much better than commercial LIBs.^[10–13] Nevertheless, Li–S batteries still face several significant challenges.^[14] In particular, the huge volume change,^[15] the low electronic and ionic conductivity of sulfur, and the discharge product lithium sulfides (Li₂S) hamper the redox reaction rates, resulting in sluggish kinetics. Due to the shuttle effect^[16] caused by the high solubility of lithium

polysulfides (LiPSs) in the electrolyte, the Li–S battery's cycle performance deteriorates.

Carbon has excellent conductivity and physical adsorption properties. Nazar's^[17] group found that CMK-3 with lots of mesoporous channels combines sulfur by melting at high temperatures, which can significantly increase the specific discharge capacity of sulfur. This major breakthrough triggered an upsurge in Li–S batteries research on carbon materials. In particular, carbon hollow spheres have attracted considerable interest due to their available cavities and high specific surface areas. For instance, Archer^[18] and co-workers fabricated highly graphitized carbon hollow spheres as a sulfur host material with special surface areas of 648 m² g⁻¹ and a pore size of 3 nm, demonstrating a capacity of 974 mAh g⁻¹ after 100 cycles at a current density of 0.5 C, but only presenting 450 mAh g⁻¹ at a current density of 3 C. This indicates that the carbon hollow sphere alone may not adequately address the slow LiPS conversion kinetics, particularly at high current density.

It has been reported that transition metal oxides have polar surfaces because of their unique electronic structures. They can interact with polar lithium polysulfides.^[19–21] As special metal oxides, bimetallic oxides often have strong conductivity and electrochemical activity.^[22,23] For example, Ze Zhang^[24] reported that Ni–Fe bimetallic oxide (NiFe₂O₄) nanoparticles were stably and uniformly grown on carbon nanotubes as an electrocatalyst sulfur host material for Li–S batteries with long cycle life. It has a specific capacity of 550 mAh g⁻¹ at a current density of 5 C, and the capacity fade rate of each cycle is 0.029% in 1000 cycles at a current density of 1 C.

Although monometallic oxide such as Co^[25], V^[26] was reported in detail, less research reports on the application of Co–V bimetallic oxide in Li–S batteries. Therefore, we have

[a] J. Zhang, M. Xiao, W. Du, J. Feng, Q. Xiang, Y. Meng, F. Zhu
School of Materials Science and Engineering, Lanzhou University of Technology, Lanzhou 730050, China
E-mail: xiaojm@lut.edu.cn
chzfl@126.com

[b] M. Xiao, Y. Meng, F. Zhu
State Key Laboratory of Advanced Processing and Recycling of Non-ferrous Metals, Lanzhou 730050, China

 Supporting information for this article is available on the WWW under <https://doi.org/10.1002/batt.202400310>

prepared a carbon hollow sphere (C-HS) composite uniformly composed of Co–V bimetallic oxide named CoVO/C-HS. It has high reaction kinetic and catalytic and can be used to achieve great performance in long time life and high current density. The adsorption experiment has proven that the shuttle effect could be alleviated by CoVO/C-HS, which can improve capacity retention further. With ~75% sulfur loading, the cathode provides a specific capacity of $1237.2 \text{ mAh g}^{-1}$ at current density of 0.2 C and holds at 603 mAh g^{-1} after 100 cycles. At high current density, its specific capacity is 976.2 mAh g^{-1} . After 1000 cycles, it leaves 338.3 mAh g^{-1} , and the capacity retention rate of each cycle is 99.89%.

2. Results and Discussion

Figure 1 shows the preparation process of CoVO/C-HS. We use SiO_2 nanoparticles as the hard template of C-HS. The phenolic

resin generated by the polycondensation of resorcinol and formaldehyde under alkaline conditions is used as the carbon source.^[27] The preparation of CoVO/C-HS needs to drop add NH_4VO_3 solution and CoCl_2 solution during the polycondensation, and the resulting precursors will be mixed into the phenolic resin. This process can improve adhesion and dispersion. Then, phenolic resin was carbonized at a high temperature, and the SiO_2 template was removed in NaOH solution. On the one hand, the polar surface of $\text{Co}_3\text{V}_2\text{O}_8$ can adsorb polysulfides and inhibit the shuttle effect.^[28] On the other hand, $\text{Co}_3\text{V}_2\text{O}_8$ is an electro-catalyst that catalyzes the conversion of lithium polysulfide, which helps to improve the reaction kinetics.^[29]

We analyzed the sample morphology using SEM and TEM. Figures 1b and c are the SEM images of C-HS and CoVO/C-HS, respectively. We found that both samples were size uniform balls, and particle size statistics show the size was ~340 nm. The TEM images (Figures 1d and e) further illustrate the CoVO/C-HS

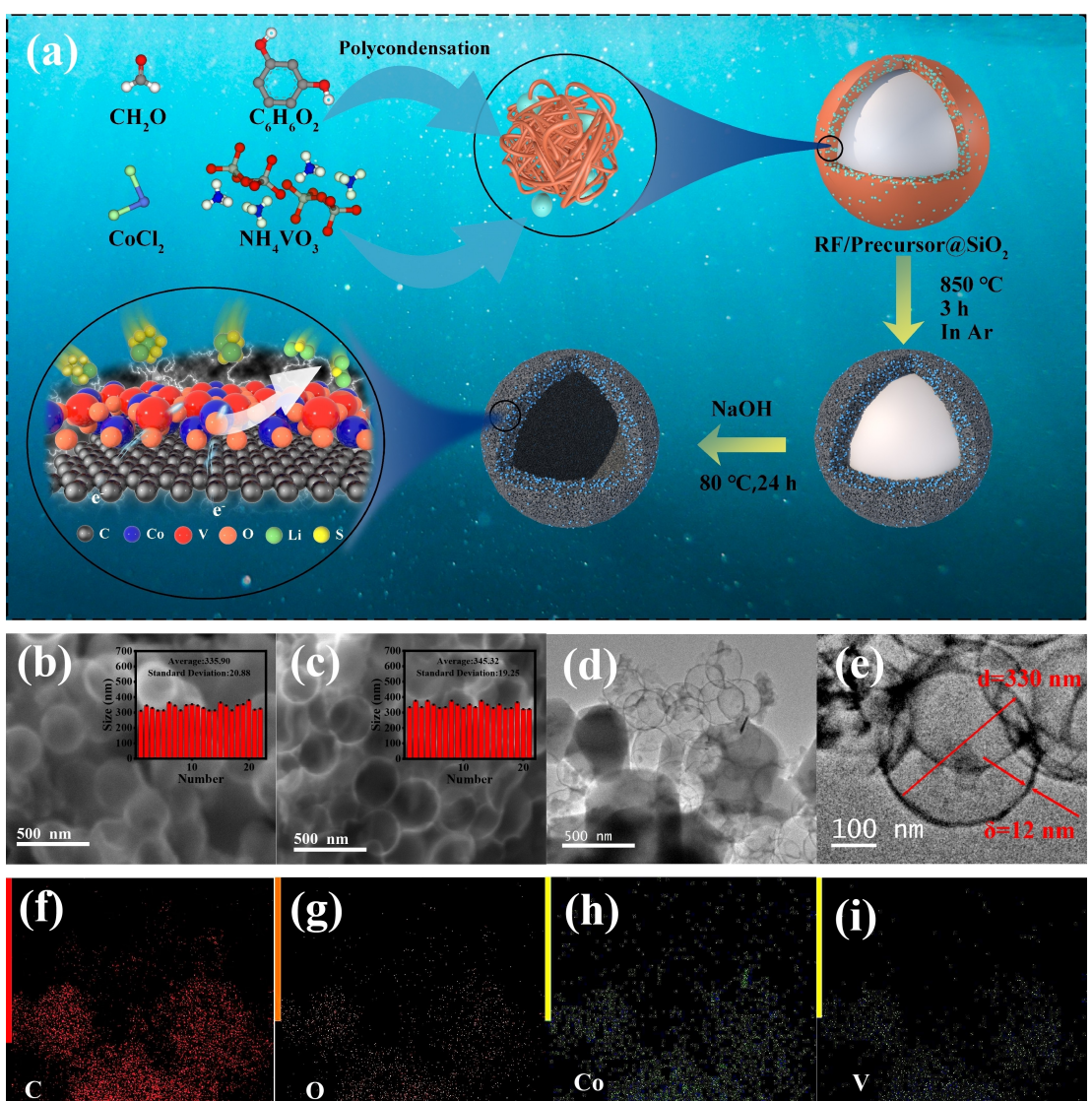


Figure 1. (a) Schematics show the synthesis process of CoVO/C-HS and its operational mechanism at the bottom left corner, (b) SEM images of C-HS and (c) CoVO/C-HS, inset shows the particle size statistics, (d, e) TEM images of CoVO/C-HS, (f-i) mapping images of CoVO/C-HS.

hollow structure, which has 320 nm hollow and 12 nm layer thickness. The hollow structure can pack more sulfur and hinder the diffusion of lithium polysulfide by the composite carbon layer. Element mapping (Figures 2f–i) shows that the sample has C, O, Co, and V and is dispersed evenly. The dispersion situation is consistent with the TEM morphology. Further, we can clearly find peaks for O and V in the EDS spectrum of the sample (Figure S1). Thought the Quantitative analysis of Co and V elements that the atomic number ratio is 3.37:1.87, which is close to the atomic number ratio in $\text{Co}_3\text{V}_2\text{O}_8$, further supporting the successful synthesis of the sample. Figure S2 shows the TEM and element mapping image of CoVO/C-HS@S. The light-colored part before loading sulfur turned into a dark color, and the S element distribution was consistent with its TEM image, proving that S was contained in the hollow.

We use X-ray diffraction (XRD) for material characterization. In the XRD patterns of C-HS and CoVO/C-HS (Figure 2a), we can find the broad peak at 24° of 2θ is attributed to the (002) crystal plane of amorphous carbon because of C-HS. Compared with C-HS, the XRD patterns of CoVO/C-HS have obvious diffraction peaks at 29.6° and 33.5° . We find (200) and (220) crystal planes in standard PDF card PDF#37-0352.^[30] The two are consistent. The XPS test is used to analyze the valence state of the element further to determine the composition of the substance. C, Co, V,

O, and N were detected in the XPS total spectrum (Figure 2b). Figure 2c was the high-resolution XPS spectrum of sample Co 2p. It consists of four characteristic peaks at 780.8 eV, 786.9 eV, 795.8 eV, and 800.3 eV, corresponding to Co^{2+} 2p_{3/2} and Co^{2+} 2p_{1/2} and its satellite features, respectively. Figure 2d is the high resolution XPS pattern of V 2p of the sample. It consists of two peaks at 526.5 eV and 517 eV, corresponding to V^{5+} 2p_{3/2} and V^{5+} 2p_{1/2}, respectively. Figure 2e is the high-resolution XPS pattern of the sample C 1s, consisting of characteristic peaks at 287.5 eV, 285.9 eV, and 284.8 eV. Figure 2f shows the high-resolution XPS pattern of the sample O 1s. It consists of three peaks located at 530.6 eV and 532.1 eV, corresponding to V–O and Co–O, respectively. The results of the XPS pattern are consistent with the valence states of the elements of $\text{Co}_3\text{V}_2\text{O}_8$ in the sample, which prove successful synthesis.^[28] Figures 2g and h analyses the pore distribution in the carbon layer and specific surface area of C-HS and CoVO/C-HS. The specific surface area and average pore volume of C-HS were $624.9 \text{ m}^2 \text{ g}^{-1}$ and $0.738 \text{ cm}^3 \text{ g}^{-1}$, while those of CoVO/C-HS were $70.01 \text{ m}^2 \text{ g}^{-1}$ and $0.12 \text{ cm}^3 \text{ g}^{-1}$. The specific surface area and pore volume of CoVO/C-HS were reduced compared with C-HS, but it still retains a microporous structure. This may be related to the fact that CoVO occupies part of the pore volume in the carbon layer after carbonization, thereby reducing the surface area of the

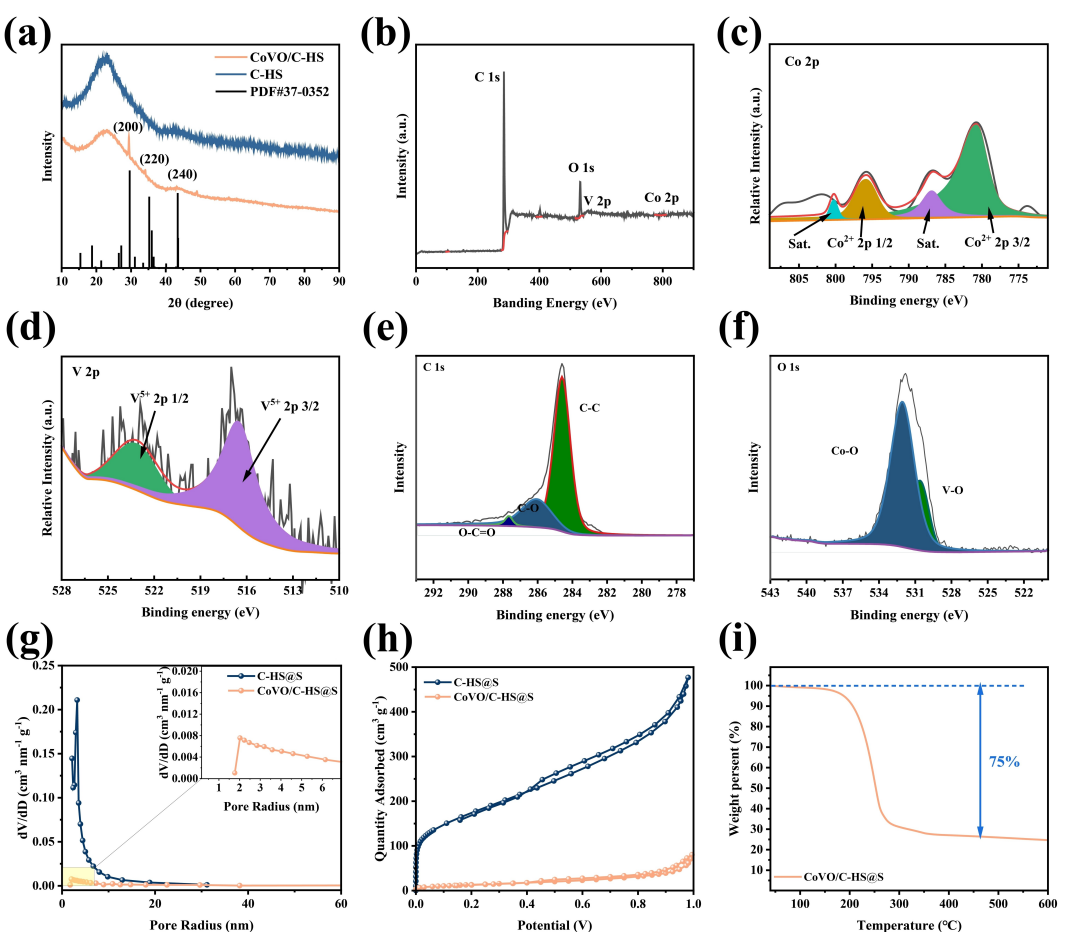


Figure 2. (a) XRD patterns of the C-HS and CoVO/C-HS; (b) XPS spectra and high-resolution XPS spectra of (c) Co 2p, (d) V 2p, (e) C 1s and (f) O 1s; (g) porous distribution and (h) N_2 adsorption-desorption isotherm of C-HS and CoVO/C-HS; (i) TGA curve of CoVO/C-HS@S.

sample and pore volume. At the same time, some studies^[31,32] have pointed out that adding Co ions in the synthesis of phenolic resin can increase the residual carbon rate after carbonization. The increase in residual carbon rate will also lead to the dense structure of carbonized materials and reduce the specific surface area and porosity of materials. Figure 2i shows the thermogravimetric (TG) curve of CoVO/C-HS@S. As the temperature rises, the sulfur begins to sublime, the sample weight loss rate begins to accelerate after 200 °C, the weight loss rate begins to slow down at about 275 °C, and the sample quality stabilizes at about 400 °C finally. The total mass loss of the whole process is about 75%, and the weight loss is due to the sublimation of sulfur.

In order to prove the excellent electrochemical reaction kinetics of CoVO/C-HS, electrochemical tests, as shown in Figure 3. The CV curves, as shown in Figure 3a, can determine the potential and intensity of electrochemical reactions and reflect the kinetics further. We can find two oxidation peaks in the CV curves of CoVO/C-HS compared with C-HS. They represent the oxidation of Li₂S to soluble lithium polysulfide (2.36 V) and further oxidation to S₈ (2.41 V), while C-HS@S only shows one oxidation peak due to slow kinetics.^[33] At the same time, smaller voltage difference between oxidation and reduction reactions of CoVO/C-HS@S. Through the CV curves at

different scan speeds, the battery dynamics and macroscopic lithium ion diffusion coefficient can be further analyzed. Figures 3d–f shows the reaction current versus the square root of the scan rates. Apply the Randles-Sevcik^[34–36] equation to calculate the Li⁺ diffusion coefficient, which as shown in Equation (1)

$$I_p = 2.687 \times 10^5 n^{1.5} A D_{Li}^{0.5} v^{0.5} c_{Li} \quad (1)$$

where n is the number of charge transfers, A is the area of the electrode, v is the scan rate, and c_{Li} is the concentration of Li⁺. The slope of the straight line is positively related to the diffusion coefficient of lithium ions. In the different reaction stages, the Li⁺ diffusion coefficient of CoVO/C-HS is always faster than that of C-HS. The rapid movement of lithium ions speeds up the battery reaction.

Figure 3g shows the electrochemical impedance spectroscopy (EIS) of the C-HS and CoVO/C-HS, and the inset is the circuit diagram of the impedance. From the equivalent circuit diagram in the inset, the impedance R_{ct} in the medium frequency of the EIS spectrum represents the charge transfer impedance.^[37,38] By fitting the EIS spectrum, the R_{ct} of COVO/C-HS is smaller than C-HS, and the reduction in charge transfer impedance symbolizes the reduction in the difficulty of inter-

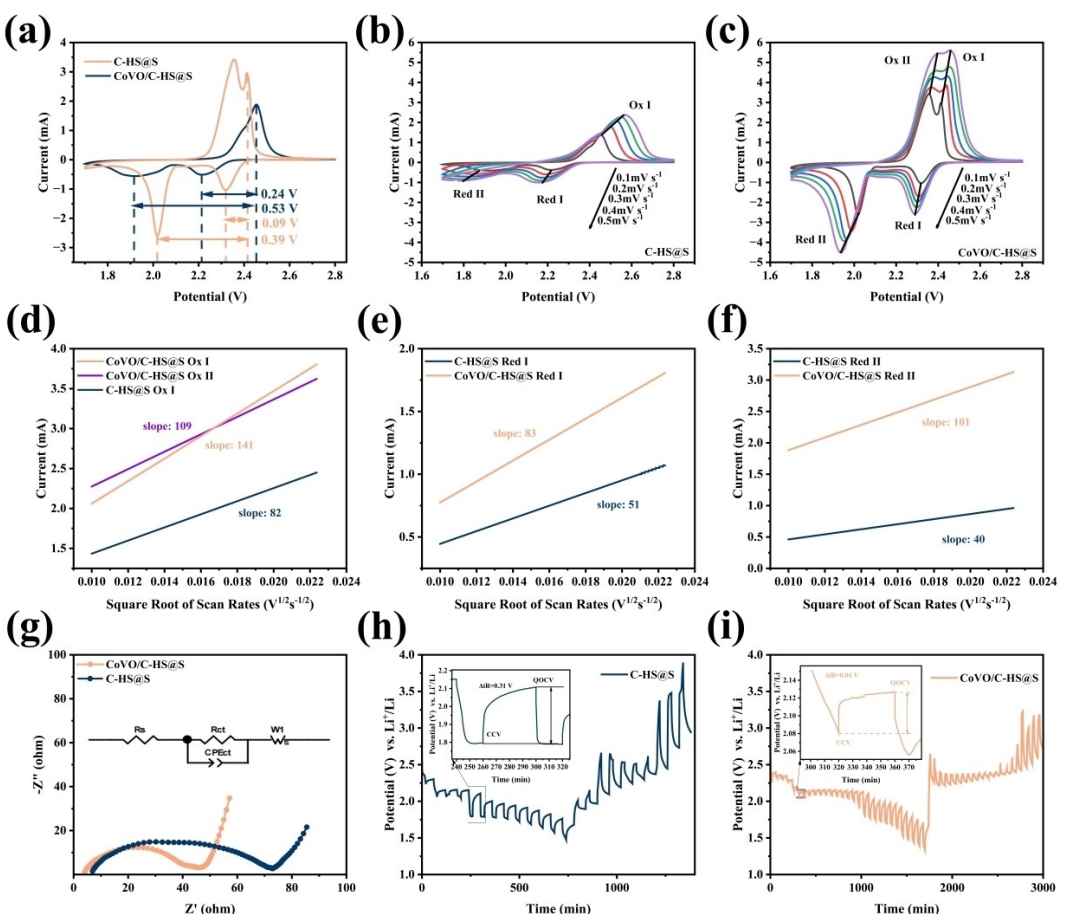


Figure 3. (a) CV curves of C-HS@S and CoVO/C-HS@S at a scanning rate of 0.1 mV s⁻¹; (b) CV curves at different scan rates of C-HS@S and (c) CoVO/C-HS@S; (d–f) reaction current of oxidation and reduction process versus the square root of the scan rates; (g) EIS (the inset is the circuit diagram of impedance); (h) GITT curves of C-HS@S and (i) CoVO/C-HS@S

face charge transfer. It facilitates the occurrence of lithium-sulfur battery reactions.^[39,40]

The GITT test is often used to calculate the lithium ion diffusion coefficient and the kinetic performance.^[41–43] The internal resistance (ΔR_{Ω}) can be quantified according to the equation $\Delta R_{\text{internal}} = |\Delta V_{\text{QOCV-CCV}}| / I_{\text{applied}}$. Here, $\Delta V_{\text{QOCV-CCV}}$ is the voltage difference between the points of quasi-open-circuit-voltage and closed-circuit-voltage, and I_{applied} is the current applied. As shown in Figures 3h and i, the internal resistance of CoVO/C-HS at the Li_2S nucleation point is much smaller than that of C-HS, indicating that its polarization is smaller and the reaction kinetics of transforming LiPSs is faster.^[44]

To verify the catalytic function of CoVO/C-HS, the Tafel plots of the reduction peak (at ~ 2.3 V, which is about S_8 to Li_2Sn , and ~ 2.0 V, which is about Li_2S_n to Li_2S) and oxidation peak (at ~ 2.4 V for Li_2S to Li_2S_n) are presented in Figures 4a–c. For the reduction process, the fitted Tafel slopes of the C-HS and CoVO/C-HS are 55 and 49 mV dec⁻¹, respectively. The fitted slopes of the Tafel slopes of the C-HS and CoVO/C-HS at the oxidation process are 116 and 79 mV dec⁻¹. The steeper the slopes of Tafel, the stronger the catalytic activity. So, CoVO/C-HS has a bifunctional catalytic effect for the rapid conversion between LiPSs and Li_2S .^[45]

In the symmetrical battery test, the anode and cathode are the same, which can eliminate the influence of lithium and directly reflect the catalytic effect of the electrode. It can be cleanly seen from the CV curve in Figure 4d that the conversion of Li_2S_6 has a more obvious current response by CoVO/C-HS, which proves that it has a better catalytic effect. As shown in Figures 4e, f in the Li_2S deposition experiment, the capacity of the precipitated is 329 mAh g^{-1} on CoVO/C-HS, which is higher than that on C-HS (277 mAh g^{-1}). The peak current appears earlier (211 s), so the nucleation of Li_2S is also easier. The improvement of Li_2S deposition kinetics not only increases the capacity of the battery but also deposits and anchors the soluble polysulfide lithium and reduces the shuttle effect.^[46] Figure 4g shows the constant pressure decomposition of Li_2S . Compared with C-HS, CoVO/C-HS produces a stronger current response, proving that it also has a catalytic effect on the oxidation of Li_2S .^[47] The bifunctional catalytic effect was demonstrated.

Figure 4h shows the UV-Vis absorption spectra of the solution after standing for 12 hours in the adsorption experiment, and the inset shows the solution after standing. It can be seen that the solution with CoVO/C-HS has the lightest color, which proves that it has good adsorption properties for LiPSs.

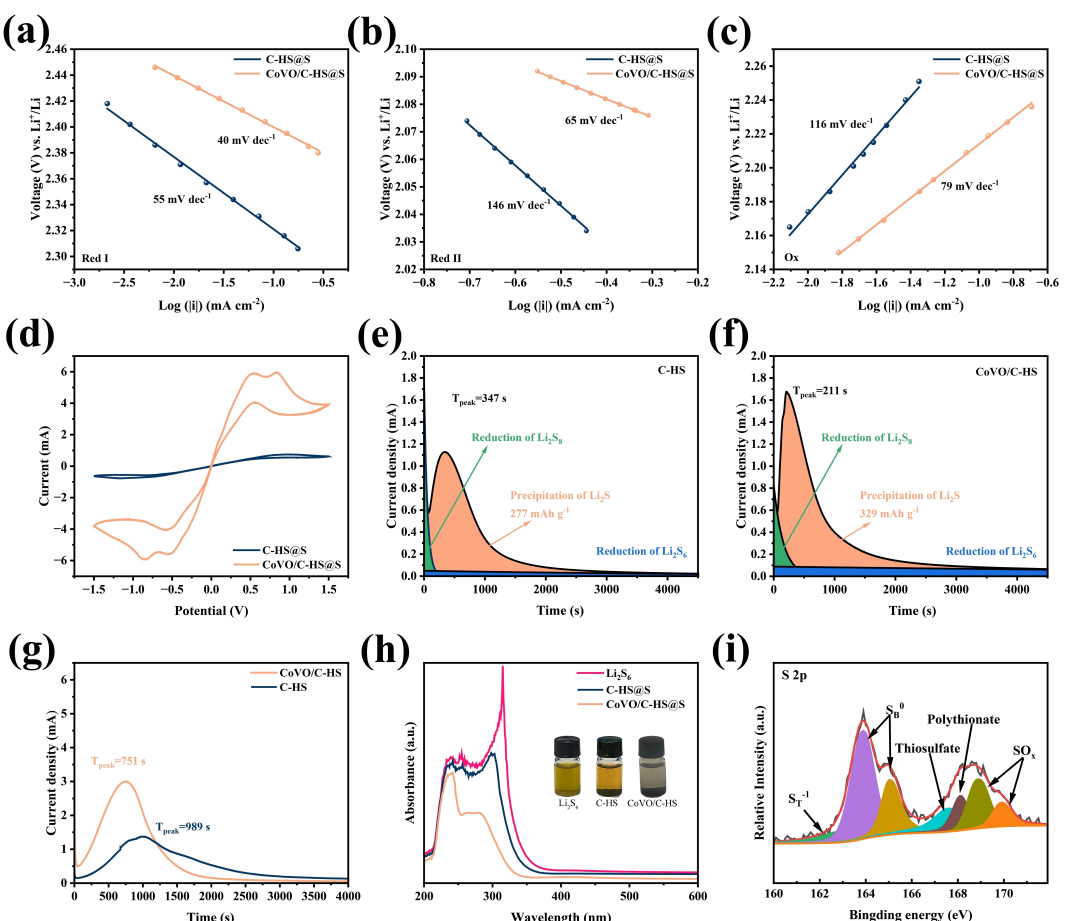


Figure 4. (a) Tafel plots calculated from the reduction peak at ~ 2.3 V, (b) ~ 2.0 V, and (c) oxidation peak at ~ 2.4 V; (d) CV curve of symmetric cell with Li_2S_6 electrolyte, Li_2S deposition experiment of (e) C-HS and (f) CoVO/C-HS, (g) constant pressure decomposition of Li_2S with C-HS and CoVO/C-HS, (h) UV-VIS absorption spectra and inset is electrolyte after standing 12 h, (i) high-resolution XPS pattern of CoVO/C-HS after absorbed Li_2S_6 .

In the UV-Vis absorption spectra, the solution curve that added CoVO/C-HS showed that the Li_2S_6 characteristic peak at 300 nm was the smallest, indicating the concentration of Li_2S_6 was lowest in the solution.^[48] The excellent adsorption properties of CoVO/C-HS were demonstrated. XPS test was performed on the CoVO/C-HS after adsorbed Li_2S_6 . Its high-resolution XPS pattern of S is shown in Figure 4i and Figure S2. After adsorption, Li_2S_6 was catalyzed to thiosulfate and polythionate for chemical adsorption. At the same time, we can find the peaks that represent the terminal (S_T^{-1}) and bridging sulfur (S_B^0) atoms of Li_2S_6 .^[28] In Figures S3a, and b, the high-resolution XPS pattern of O and Li has more new peaks about Li–O. Co did not change before and after LiPSs adsorption by obvious Figure S3c. By analyzing the high-resolution XPS pattern of V, we found V^{4+} characteristic peaks, which were considered to have contributed to the creation of thiosulfate and polythionate.^[29]

Figure 5a illustrates the galvanostatic discharge-charge curves of C-HS@S and CoVO/C-HS@S to probe the effectiveness of Li–S batteries. The CoVO/C-HS@S delivers a higher specific capacity of 1329.7 mAh g^{-1} than C-HS@S (921.1 mAh g^{-1}). This is because the lower difference between the charge and discharge plateau of CoVO/C-HS@S (177 mV) specific capacity is affected by decreased polarization. This was attributed to the higher utilization of sulfur through the catalytic effect of $\text{Co}_3\text{V}_2\text{O}_8$ in electrochemical reactions. Further, Figure 5b shows the 100 cycles of discharge data at a current density of 0.2 C. Great cycling stability was achieved, and CoVO/C-HS@S delivered an initial specific capacity of 1237.2 mAh g^{-1} . After 100 cycles, the specific discharge capacity can still maintain above 603 mAh g^{-1} , and the coulombic efficiency of each cycle is nearly 100%. However, C-HS@S initially only had a specific capacity of 786.9 mAh g^{-1} . After 100 cycles, the specific

discharge capacity is only at 318.1 mAh g^{-1} . At a high current density of 2 C, CoVO/C-HS showed an initial specific capacity of 976.2 mAh g^{-1} . After 1000 cycles, it still maintained 338.3 mAh g^{-1} . The capacity retention rate per cycle was 99.89%. The initial specific capacity of C-HS@S was 665 mAh g^{-1} ; after 1000 cycles, it is 132.3 mAh g^{-1} . In the long cycle performance test under different current densities, CoVO/C-HS showed greater improvement than C-HS. Specific capacities of 855.3 mAh g^{-1} , 728 mAh g^{-1} , 660.5 mAh g^{-1} , and 574.3 mAh g^{-1} are realized at current densities of 0.2 C, 0.5 C, 1 C, and 2 C, respectively and shown in Figure 5e. They are obviously superior to the C-HS@S electrode. After cycling at a higher current density, the specific capacity could track back to 764 mAh g^{-1} when the current density returned to 0.2 C. It demonstrates that capacity has reversibility and CoVO/C-HS@S has a stable structure.

In order to explain more about the mechanism by which C-HS and CoVO/C-HS adsorbed LiPSs, we carried out density functional theory (DFT) with corrections for van der Waals forces. We selected (200) crystal faces, which were specific in XRD as the exposed surface. We made the binding geometries large over 2 nm to eliminate the interaction between molecules. The binding energy E_b can be calculated by Equation (2):

$$E_b = E_{\text{sub+LiPS}} - E_{\text{LiPS}} - E_{\text{sub}} \quad (2)$$

The result of binding energy is shown in Figure 6a and compared in Figure 6b. CoVO/C-HS can provide stronger binding energy and is able to immobilize lithium polysulfide molecules on the cathode side, which can alleviate the shuttle effect. There is a huge difference between the two binding

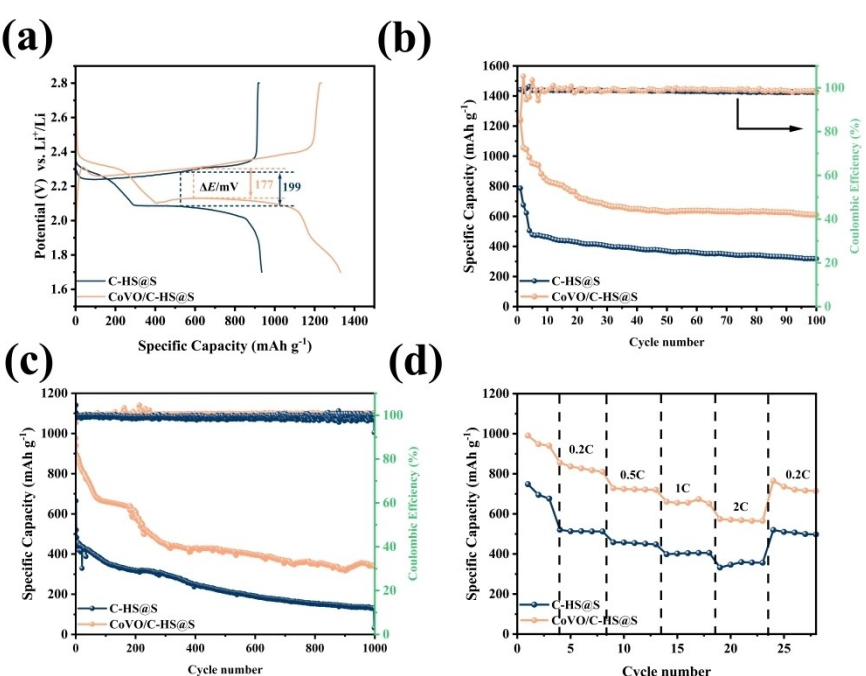


Figure 5. (a) galvanostatic discharge-charge curves of C-HS@S and CoVO/C-HS@S, (b) discharge data at current density of 0.2 C about C-HS@S and CoVO/C-HS@S, (c) discharge data at current density of 2 C, (d) specific capacities at current densities of 0.2 C, 0.5 C, 1 C, 2 C.

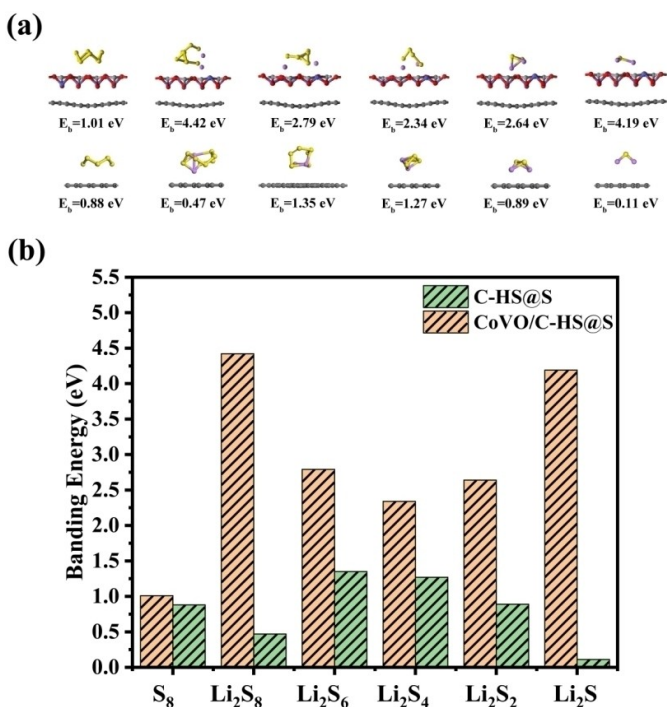


Figure 6. (a) LiPSs adsorption energy of C-HS and CoVO/C-HS, (b) bar chart of binding energy.

energies for Li_2S_8 . This is because the nonpolar surface of C-HS cannot provide strong binding energy, but CoVO/C-HS can.

3. Conclusions

In this work, we successfully made CoVO/C-HS with a high sulfur loading ratio of 75%. Because of the particularity of the process, $Co_3V_2O_8$ has good dispersion in the carbon layer. Due to the exposed polar surface, CoVO/C-HS is able to interact strongly with lithium polysulfide. The CV curve and EIS spectrum indicate that it has faster battery reaction kinetics than C-HS, which can speed up the battery reaction and increase the battery capacity. Further, deposition and decomposition experiments of Li_2S and Li_2S_6 adsorption experiments verified the excellent catalytic effect and adsorption of lithium polysulfide by CoVO/C-HS. Thanks to these excellent electrochemical properties, when it is used in lithium-sulfur battery cathode sulfur host materials at a sulfur loading of 75%, the initial capacity is $1237.2 \text{ mAh g}^{-1}$ at a current density of 0.2 C and remains at 603 mAh g^{-1} after 100 cycles. With a high current of 2 C, the initial capacity is 976.2 mAh g^{-1} , the retention rate per cycle is 99.89%, and it is stable for 1,000 cycles. Under changes in current density, the capacity is reversible, showing good battery stability and indicating its huge potential in lithium-sulfur battery applications.

Supporting Information Summary

Additional supporting information can be found online in the Supporting Information section at the end of this article.

Declaration of Competing Interest

The authors declare that they have no known competing financial interests or personal relationships that could have appeared to influence the work reported in this paper.

Author Contributions

Mingjun Xiao, Yanshuang Meng, and Fuliang Zhu guided all the experimental design and led the manuscript preparation and revision work. Jiangnan Zhang, Wei Du, Jiawei Feng, and Qiang Xiang did most of the experiments and data analysis. All of the authors have approved the final version of the manuscript.

Acknowledgements

This work was supported by the National Natural Science Foundation of China (52064035), the Key Research and Development Program of Gansu Province (22YF7GA157), the Natural Science Foundation of Zhejiang Province (LGG22E020003), the Science and Technology Program of Gansu Province (24JRRRA193), and the Doctoral Research Foundation of Lanzhou University of Technology in 2023 (062316).

Conflict of Interests

The authors declare no conflict of interest.

Data Availability Statement

Data will be made available on request.

Keywords: $Co_3V_2O_8$ • Carbon hollow spheres • Catalyze • Lithium-sulfur batteries

- [1] Y. Wang, X. Han, L. Lu, X. Feng, J. Li, M. Ouyang, *Automot. Eng.* **2022**, 44 (4), 617–637.
- [2] L. Ding, *Chin. J. Power Sources* **2015**, 39 (8), 1780.
- [3] D. Xu, *Electr. Power* **2004**, 37 (9), 1–4.
- [4] H. Xu, G. Shao, E. Chunliang, J. Guo, *Power Gener. Technol.* **2023**, 44 (4), 484–491.
- [5] X. Yu, X. Xu, S. Chen, J. Wu, H. Jia, *Trans. China Electrotech. Soc.* **2016**, 31 (1), 1–13.
- [6] S. Ma, Y. Zhang, X. Liu, *J. Detect. Control* **2023**, 45 (4), 29–34.
- [7] B. Xu, W. Liu, *Battery* **2002**, 32 (4), 242–244.
- [8] J. Zhang, W. Tong, H. Qi, *Chin. J. Power Sources* **2017**, 41 (9), 1377–1379.
- [9] Z. Zhang, *J. Electrochem.* **2015**, 21 (3), 299–301.
- [10] X. Jia, *Chin. J. Power Sources* **2014**, 38 (9), 1765–1767.

- [11] S. Liu, L. Yao, Q. Zhang, L.-L. Li, N.-T. Hu, L.-M. Wei, H. Wei, *Acta Physico-Chimica Sinica* 2017, 33 (12), 2339–2358.
- [12] H. Pang, Z. Chen, F. Ding, X. Liu, *Chin. J. Power Sources* 2016, 40 (8), 1715–1717 (1740).
- [13] T. Tang, L. Zhang, Z. Guo, X. Gu, *Chin. J. Rare Metals* 2022, 46 (7), 954–964.
- [14] J. J. Hu, G. R. Li, X. P. Gao, *J. Inorg. Mater.* 2013, 28 (11), 1181–1186.
- [15] L. Wen, J. Liang, Y. Shi, J. Chen, Z. Sun, M. Wu, F. Li, *Energ. Stor. Sci. Technol.* 2018, 7 (3), 465–470.
- [16] S. Gu, J. Jin, Y. Lu, R. Qian, Z. Wen, *Ener. Stor. Sci. Technol.* 2017, 6 (5), 1026–1040.
- [17] X. L. Ji, K. T. Lee, L. F. Nazar, *Nat. Mater.* 2009, 8 (6), 500–506.
- [18] N. Jayaprakash, J. Shen, S. S. Moganty, A. Corona, L. A. Archer, *Angew. Chem. Int. Ed.* 2011, 50 (26), 5904–5908.
- [19] P. Hui, R. Yang, Q. Deng, Y. Yan, Y. Xu, *Chemistry* 2019, 82 (11), 982–988.
- [20] X. Liu, J. -Q. Huang, Q. Zhang, L. Mai, *Adv. Mater.* 2017, 29 (20), 1601759.
- [21] X. Tao, J. Wang, C. Liu, H. Wang, H. Yao, G. W. Zheng, Z. Seh, Q. Cai, W. Li, G. Zhou, C. Zu, Y. Cui, *Nat. Commun.* 2016, 7, 11203.
- [22] Y. Chen, J. Li, X. Kong, Y. Zhang, Y. Zhang, J. Zhao, *ACS Sustainable Chem. Eng.* 2021, 9 (30), 10392–10402.
- [23] X. Zhang, Y. Fan, M. A. Khan, H. Zhao, D. Ye, J. Wang, B. Yue, J. Fang, J. Xu, L. Zhang, J. Zhang, *Batteries & Supercaps* 2020, 3 (1), 108–116.
- [24] Z. Zhang, S. Basu, P. Zhu, H. Zhang, A. Shao, N. Koratkar, Z. Yang, *Carbon* 2019, 142, 32–39.
- [25] W. Ren, W. Ma, M. M. Umair, S. Zhang, B. Tang, *ChemSusChem* 2018, 11 (16), 2695–2702.
- [26] J. N. Zhang, M. J. Xiao, T. T. Liu, Y. S. Meng, F. L. Zhu, Z. Y. Fan, *Green Chem.* 2024.
- [27] H. Wei, C. Wag, H. Wang, *China Plastics Industry* 2003, 31 (2), 16–18.
- [28] J. Sivaraj, B. Dasari, K. Ramesha, *Energ. Fuego At.* 2023, 37 (13), 9672–9681.
- [29] L. Zhang, F. Wan, H. Cao, L. Liu, Y. Wang, Z. Niu, *Small* 2020, 16 (18), 1907153.
- [30] Y. J. Zhang, Y. Y. Liu, J. Chen, Q. F. Guo, T. Wang, H. Pang, *Sci. Rep.* 2014, 4, 5687.
- [31] X. Zhang, X. Chen, Z. Li, P. Guo, Y. Han, Y. Jia, S. Gao, *Chem. Res. Appl.* 2020, 32 (8), 1409–1414.
- [32] Z. Lei, Y. X. Yan, W. G. Fei, *J. Funct. Polym.* 2011, 34 (01), 18–22.
- [33] M. Cuisinier, P. E. Cabelguen, S. Evers, G. He, M. Kolbeck, A. Garsuch, T. Bolin, M. Balasubramanian, L. F. Nazar, *J. Phys. Chem. Lett.* 2013, 4 (19), 3227–3232.
- [34] D. Li, L. Dai, X. Ren, F. Ji, Q. Sun, Y. Zhang, L. Ci, *Energy Environ. Sci.* 2021, 14 (1), 424–436.
- [35] T. L. Nguyen, T. N. Vo, V. D. Phung, K. Ayalew, D. Chun, A. T. Luu, Q. H. Nguyen, K. J. Kim, I. T. Kim, J. Moon, *Chem. Eng. J.* 2022, 446, 137174.
- [36] A. Ottmann, G. S. Zakharova, B. Ehrstein, R. Klingeler, *Electrochim. Acta* 2015, 174, 682–687.
- [37] Z. Deng, Z. Zhang, Y. Lai, J. Liu, J. Li, Y. Liu, *J. Electrochem. Soc.* 2013, 160 (4), A553–A558.
- [38] S. D. Talian, J. Moskon, R. Dominko, M. Gaberscek, *Adv. Mater. Interfaces* 2022, 9 (8), 2101116.
- [39] S.-Z. Xiong, K. Xie, X.-B. Hong, *Chem. J. Chinese U.-Chinese* 2011, 32 (11), 2645–2649.
- [40] R. Xu, I. Belharouak, X. Zhang, R. Chamoun, C. Yu, Y. Ren, A. Nie, R. Shahbazian-Yassar, J. Lu, J. C. M. Li, K. Amine, *ACS Appl. Mater. Interfaces* 2014, 6 (24), 21938–21945.
- [41] J. W. Dibden, N. Meddings, J. R. Owen, N. Garcia-Araez, *ChemElectro-Chem* 2018, 5 (3), 445–454.
- [42] C. Long, L. Li, M. Zhai, Y. Shan, *J. Phys. Chem. Solids* 2019, 134, 255–261.
- [43] T. Zerrin, R. Shang, B. Dong, E. C. Aguilar, J. Malvin, M. Ozkan, C. S. Ozkan, *Nano Energy* 2022, 104, 107913.
- [44] J. Wei, H. Su, C. M. Qin, B. Chen, H. Zhang, J. M. Wang, *J. Electroanal. Chem.* 2019, 837, 184–190.
- [45] L. Y. Tian, Z. Zhang, S. Liu, G. R. Li, X. P. Gao, *Nano Energy* 2023, 106, 108037.
- [46] F. Y. Fan, W. C. Carter, Y.-M. Chiang, *Adv. Mater.* 2015, 27 (35), 5203–5209.
- [47] F. C. Han, F. J. Li, L. Chen, L. Y. He, Y. A. Jiang, S. D. Xu, D. Zhang, L. Qi, *Chem. J. Chinese U.* 2022, 43 (8).
- [48] N. Xu, M. Wang, T. Qian, C. Yan, *Energy Storage Sci. Technol.* 2017, 6 (3), 522–528.

Manuscript received: May 8, 2024

Revised manuscript received: June 6, 2024

Accepted manuscript online: July 9, 2024

Version of record online: August 23, 2024